Simultaneous adsorption of ammonia and phosphate using ferric sulfate modified carbon/zeolite composite from coal gasification slag

Simultaneous adsorption of ammonia and phosphate using ferric sulfate modified carbon/zeolite composite from coal gasification slag

Xianyao Ma[1,2,3], Yingxue Li[4], Defu Xu[1,2,3*], Hanxin Tian[1,2,3], Hong Yang[5*]

[1]*Collaborative Innovation Center of Atmospheric Environment and Equipment Technology, Nanjing 210044, China;*

[2]*Jiangsu Key Laboratory of Atmospheric Environment Monitoring and Pollution Control, Nanjing 210044, China;*

[3]*School of Environmental Science and Engineering, Nanjing University of Information Science &Technology, Nanjing 210044, China;*

[4]*School of Applied Meteorology, Nanjing University of Information Science &Technology, Nanjing 210044, China;*

[5]*Department of Geography and Environmental Science, University of Reading, Reading, RG6 6AB, UK*

ABSTRACT

Removal of nutrients in water is crucial to control eutrophication. Fly ash has been increasingly used to synthesize zeolite to remove nutrients, but it is still poorly understood about the removal capacity of zeolite synthesized from coal gasification slag (CGS), which has not been well recycled in many countries. In this study, the CGS was acid leached, alkali dissolved, and synthesized to carbon/zeolite composite (C/ZC) under induction by medical stone. After being modified by ferric sulfate, the composite was analyzed for the adsorption of NH_4^+ and PO_4^{3-}. Results showed that the maximum adsorption capacity by C/ZC is 5.17 mg/g, but C/ZC has no adsorption capacity of PO_4^{3-}. The ferric sulfate was used to modify C/ZC to obtain carbon/zeolite composite modified by iron (M-C/ZC). M-C/ZC has a higher specific surface area (348.3 m^2/g), and the negatively charge of M-C/ZC can adsorb NH_4^+ and form Fe-O-P between PO_4^{3-} and Fe-OH bonds. The maximum adsorption capacity of NH_4^+ and PO_4^{3-} by M-C/ZC are 7.44 mg/g and 6.94mg/g, respectively. The removal efficiency of NH_4^+ and PO_4^{3-} are up to 88% and 99% under initial NH_4^+ (5 mg/L) and PO_4^{3-} (10 mg/L) concentration. The regeneration capacity of M-C/ZC of NH_4^+ was stronger than that of PO_4^{3-}. After three cycles, the regeneration rate of M-C/ZC of NH_4^+ was still up to 76.96%. Our findings suggest the good application potential of M-C/ZC for removing NH_4^+ and PO_4^{3-} from wastewater.

Keywords: Coal gasification slag, zeolite, ammonia nitrogen, phosphate, iron modification

* Corresponding authors, Tel. 0086-025-58695684 Fax. 0086-025-58731089 E-mail. defuxu1@163.com (D. Xu); hongyanghy@gmail.com (H. Yang)

1. Introduction

Water eutrophication not only impacts the aquatic ecological functions, but also affects drinking water safety and threatens human health in the world, particularly in many developing countries (Yang et al., 2012a; Yang et al., 2012b). Different methods have been developed to remove nitrogen and phosphorus, including adsorption, crystallization, ion exchange, precipitation, biological removal, and others (Li et al., 2021; Salimova et al., 2020). Among these technologies, adsorption is widely applied, because of its relatively low cost, small energy consumption, and easy implementation (Qu, 2008). Adsorbents used to adsorb nitrogen (N) or phosphorus (P) usually included activated carbon, zeolite, clay minerals, iron oxide (Fang et al., 2017; Ren et al., 2021; Wang et al., 2018). Of these adsorbents, zeolite has been increasingly used for wastewater treatment.

Natural zeolite is a non-renewable resource, so it is essential to produce synthetic zeolite for the removal of N and P from wastewater. Typical raw materials for synthetic zeolite included fly slag, kaolin, blast furnace slag, rice husk slag and others (Khaleque et al., 2020; Wang et al., 2020). Among these raw materials, fly ash (FA) synthetic zeolite has been extensively studied because of its clear molecular and porous structure, large surface area and good ion exchange performance (Petrus and Warchol, 2005). Coal is one of the most widely used primary energy sources in the world, with a large amount of by-products of FA and coal gasification slag (CGS). The FA comes from coal combustion with enough oxygen, and CGS is the solid waste in the process of coal gasification (Huo et al., 2012). The combustible part of coal reacts with oxygen and water vapor under high temperature to convert into syngas in a gasifier. The fine residue of coal gasification is the slag, which is carried out by the syngas flow through the top of the gasification furnace, passes through the black water treatment system, and then is formed by the pressure filter (Tang et al., 2018). Although FA and CGS share similar chemical element compositions, such as O, Si, Al and Fe (Appiah-Hagan et al., 2018), the physical/chemical properties of the FA and CGS are different (Li et al., 2018). The former is produced in an oxidizing atmosphere, while the latter is formed in a reducing condition. This fact indicates that the resource utilization of these two coal residues might be different due to the well-known fact that material structure determines its properties. While FA has been used as raw materials to synthesize porous materials such as zeolite (Iqbal et al., 2019), more studies are still needed for the recycling of CGS.

The conversion of FA to high-quality zeolite-based products has received wide attention (Hermassi et al., 2020). In addition, some researchers begin to explore the conversion of CGS to synthetic new materials. For example, a porous carbon-silicon composite was produced from CGS under high temperature using potassium hydroxide activation and hydrochloric acid leaching, with a surface area of 1347 m^2/g and a total pore volume of 0.69 cm^3/g (Gu and Qiao, 2019). The mesoporous glass microspheres with a specific surface area of 364 m^2/g were created from CGS, and its adsorption capacity of methylene blue reached 140.57 mg/g (Liu et al., 2019). In

addition, MCM-41 and carbon/zeolite were synthesized from by CGS, and the total surface area, the external surface area, microspore surface area, the pore volume of mesoporous and mean pore size of carbon/zeolite composite were 189.27 m^2/g, 161.43 m^2/g, 27.84 m^2/g, 0.23 cm^3/g and 5.13 nm, respectively (Wu et al., 2020). Therefore, CGS has the potential to be used to synthesize multifunctional materials.

Natural zeolite (NAT-Z) has been extensively used to adsorb ammonia nitrogen (NH_4^+), but showed a limited adsorption ability for phosphate (PO_4^{3-}) (Lin et al., 2011). In addition, scholars suggested that NAT-Z had negligible adsorption ability for reactive soluble P in water (Zhan et al., 2019), due to the negative net structural charges on the zeolite framework (Lin et al., 2011). Therefore, it is important to modify NAT-Z to increase its retention ability for phosphate. For example, aluminum was used to modify zeolite to enhance its adsorption capacity of phosphate (Gibbs and Özkundakci, 2010), but dissolved Al^{3+} is toxic to invertebrates and fish in the aquatic ecosystem (Reitzel et al., 2013). Recent studies found that the modification of zeolite with ferric salt can significantly increase its adsorption capacity of P (Liu et al., 2017). Using iron modification, the P adsorption capacity of NAT-Z was improved from 0.355 mg/g to 0.506 mg/g (Zhan et al., 2019). Iron oxide is environmentally friendly, with a good affinity towards phosphate (Wang et al., 2016). Therefore, it is important for the development of ferric salt modified zeolites.

In general, about 0.2-0.3 tons of CGS is produced per ton coal gasification (Wu et al., 2020). In China, most CGS in large coal gasification projects is buried in the slag field, with very low recycling utilization rate (Gu and Qiao, 2019; Wu et al., 2020). In addition, few scholars have explored the synthetic zeolite-based products by using CGS, and it is still largely unknown for their simultaneous adsorption of NH_4^+ and PO_4^{3-}. In this study, carbon/zeolite composite is synthesized from CGS, the composite is modified by using ferric sulfate, and the adsorption of NH_4^+ and PO_4^{3-} by the composite is analyzed. The main aims of this study are 1) to develop a process to synthesize carbon/zeolite composite by using CGS; 2) to determine the simultaneous adsorption capacity of NH_4^+ and PO_4^{3-} by carbon/zeolite composite; 3) to estimate the simultaneous adsorption capacity of NH_4^+ and PO_4^{3-} by carbon/zeolite composite modified by ferric sulfate.

2. Material and Methods

2.1. Raw materials

The CGS, with an average carbon content of 37.13%, was obtained from Shanxi Xinhua Chemical Co. Ltd., Shanxi, China. Medical stone was obtained from Mengshan, Shandong, China. The main chemical components of CGS and medical stone are shown in Table 1.

2.2. Synthesis of carbon/zeolite composite

The CGS was dried in an oven at 105℃ for 24 h, passed through a 60-mesh sieve after grinding, and mixed with hydrochloric acid (28% volume fraction) in a beaker to achieve a solid-to-liquid ratio of 1:3. The solid in the beaker was separated

by centrifugation after heating in a water bath at 90℃ for 1 h, and then washed to neutral with distilled water. The washed solid was dried at 90°C for 24 h, and then ground and passed through a 60-mesh sieve to obtain acid-treated CGS.

The acid-treated CGS and 5 M sodium hydroxide solution was mixed to obtain a solid-liquid ratio of 1:5. The solution was shaken at a speed of 350 r/min under 47℃ for 6 h in a water bath stirrer. The obtained gel liquid was transferred into the reaction kettle, and medical stone through 100 mesh sieve was added to obtain the mass fraction of 5%. The reaction kettle was put into the drying oven and crystallized at 140℃ for 48 h. The solid after crystallization was washed to neutral with distilled water and dried at 105℃ for 24 h to obtain the carbon/zeolite composite (C/ZC)

2.3 Modification of carbon/zeolite composite

According to the orthogonal experiments, the C/ZC was mixed with 0.5% ferric sulfate solution with a solid-to-liquid ratio of 1:20, and then shaken at a speed of 150 r/min under 45℃ for 2 h. The solids were separated by centrifugation, and washed with distilled water. The washed solid were dried to obtain the modified carbon/zeolite composite (M-C/ZC).

2.4. Adsorption isotherm experiment of carbon/zeolite composite

Ammonium chloride and potassium dihydrogen phosphate were used to prepare the initial NH_4^+ and PO_4^{3-} at the concentrations of 5, 10, 20, 40, 80, and 160 mg/L, respectively. The pH of NH_4^+ and PO_4^{3-} solution were adjusted to 7. 0.2 g of CGS, C/ZC and M-C/ZC were added into a 100 ml polyethylene bottle, and 20 ml of different concentrations NH_4^+ or PO_4^{3-} were also added. The polyethylene bottle was shaken at 25℃ for 24 h, and centrifuged at 4000 rpm for 10 min, and an aliquot of the supernatant was filtered through a 0.45-μm filter. P in the supernatant was analyzed using the molybdenum blue-ascorbic acid method. NH_4^+ content of the subsamples was measured at the wavelength of 697 nm with a Spectrophotometer (UV-752, Shanghai Youke, China) using the salicylic acid method.

The adsorption capacities of NH_4^+ and PO_4^{3-} were calculated using the following equation (Eq. [1]):

$$q_e = \frac{(c_0 - c_e)V}{m} \qquad [1]$$

where q_e (mg/g) is the adsorbed amount of NH_4^+ or PO_4^{3-} per unit weight of CGS, C/ZC and M-C/ZC at an equilibrium concentration of adsorbate in bulk solution, respectively; V (L) is the volume of NH_4^+ or PO_4^{3-} solution; m (g) is the weight of CGS, C/ZC and M-C/ZC; C_0 (mg/L) and C_e (mg/L) are the initial and equilibrium concentrations of NH_4^+ or PO_4^{3-}.

Sorption isotherms were fitted to the Langmuir (Eq. [2]) and Freundlich (Eq. [3]) equations to quantify the adsorption capacities of the researched CGS, C/ZC and M-C/ZC.

$$q_e = \frac{q_m \cdot K_L \cdot C_e}{1 + K_L \cdot C_e} \quad [2]$$

$$q_e = K_F \cdot C_e^{\frac{1}{n}} \quad [3]$$

where q_e (mg/g) and C_e (mg/L) are the same as above; 1/n is the intensity of adsorption or affinity; q_m (mg/g) is the maximum sorption capacity; K_F (mg/g) and K_L (L/mg) are Freundlich adsorption constant and Langmuir constant.

2.5. Dosing amount adsorption experiment of carbon/zeolite composite

The pH of initial 5 mg/L NH_4^+ and 10 mg/L PO_4^{3-} were adjusted to 7. 0.05, 0.1, 0.2, 0.4 and 0.8 g of M-C/ZC were added into the 100 ml polyethylene bottle with 5 mg/L NH_4^+ or 10 mg/L PO_4^{3-}, respectively. After being shaken at 25℃ for 24 h, the suspensions were centrifuged and filtered to obtain the supernatant solution for analysis of NH_4^+ and PO_4^{3-}. The equilibrium adsorption capacities of NH_4^+ and PO_4^{3-} were calculated by using equation [1], and the removal efficiencies were calculated by using equation [4]:

$$\eta = \frac{c_0 - c_e}{c_0} \times 100\% \quad [4]$$

Where η is the removal efficiency of NH_4^+ or PO_4^{3-}, C_0 (mg/g) and C_e (mg/L) are the same as above.

2.6. Adsorption kinetics experiments of carbon/zeolite composite

0.2 g CGS, C/ZC and M-C/ZC were added to a centrifuge tube with 20 mL solution containing NH_4^+ (5 mg/L) or PO_4^{3-} (10 mg/L), which was shaken at 180 rpm in a mechanical shaker at room temperature (25 °C). Subsamples were collected after 5, 10, 20, 40, 60, 120, and 240 minutes to measure NH_4^+ and PO_4^{3-} concentrations. The amounts of NH_4^+ or PO_4^{3-} adsorbed by the adsorbents were calculated by using the following equation (Eq. [5])

$$q_t = \frac{(c_0 - c_t)V}{m} \quad [5]$$

where q_t (mg/g) is the amount of NH_4^+ or PO_4^{3-} adsorbed by the CGS, C/ZC and M-C/ZC at the given time, respectively; C_0 and C_t (mg/L) are the NH_4^+ and PO_4^3concentrations before and after adsorption time t, respectively; V (L) is the volume of adsorption solution; and m (g) is the weight of CGS, C/Z and M-C/ZC.

The experimental results were fitted to two typical kinetic models (Pseudo-first-order Eq. [6]) and Pseudo-second-order Eq. [7]).

$$\ln(q_e - q_t) = \ln q_e - k_1 t \quad [6]$$

$$\frac{t}{q_t} = \frac{1}{k_2 q_e^2} + \frac{t}{q_e} \quad [7]$$

where q_e and q_t (mg/g) are the amounts of NH_4^+ or PO_4^{3-} adsorbed by the adsorbent at the equilibrium time and the given time; k_1 (1/min) and k_2 (g/mg/min) are the rate constants of the corresponding model.

2.7. Adsorption thermodynamics of carbon/zeolite composite

0.2 g M-C/ZC was added into a polyethylene bottle with 20 mL of NH_4^+ (5 mg/L) or PO_4^{3-} (10 mg/L) at temperatures of 25℃, 35℃ and 45℃, respectively. The NH_4^+ or PO_4^{3-} was analyzed after 24 h equilibration time. The thermodynamic equilibrium constant Kc was calculated by using the following equation [8]:

$$K_c = \frac{C_0 - C_e}{C_e} \quad [8]$$

where C_o and C_e (mg/L) are the same as above.

The Gibbs free energy ΔG^o (KJ/mol), enthalpy change ΔH^o (KJ/mol) and entropy change ΔS^o (KJ/mol) were calculated by using equations [9] and [10]:

$$\Delta G^0 = -RT \ln K_c \quad [9]$$

$$\ln K_c = -\frac{\Delta G^0}{RT} = -\frac{\Delta H^0}{RT} + \frac{\Delta S^0}{R} \quad [10]$$

where T is temperature in K, R the ideal gas constant = 8.314 J/mol/K, the enthalpy (ΔH°) and entropy (ΔS°) values are calculated from the slope (ΔH°/RT) and intercept (ΔS°/R), respectively.

2.8. Effect of pH on the adsorption of ammonia nitrogen and phosphate of carbon/zeolite composite

The initial concentrations of NH_4^+ and PO_4^{3-} were 5 mg/L and 10 mg/L, respectively, and the pH of solutions were adjusted to 5, 6, 7, 8 and 9, respectively. 0.2 g M-C/ZC was added into a 100 ml polyethylene bottle with 20 mL of NH_4^+ or PO_4^{3-} solution with different pH, and the solution was shaken at the temperature of 25℃ for 24 h. The Zeta potential of the solution was determined after 24 h equilibration time, and subsamples were measured for NH_4^+ and PO_4^{3-} concentrations. The removal efficiency of NH_4^+ and PO_4^{3-} were calculated by using Equation [4].

2.9. Regeneration rates of modification of carbon/zeolite composite

To investigate the regeneration rates of M-C/ZC, M-C/ZC with saturated NH_4^+ or PO_4^{3-} was placed in a 2M NaCl solution at the solid-to-liquid ratio of 1:100. After being shaken at 25°C for 180 minutes, the concentration of NH_4^+ or PO_4^{3-} was determined in the desorption solution. In addition, M-C/ZC desorption was washed using deionized water and dried to obtain the regenerated M-C/ZC. 0.2g regenerated

M-C/ZC was added into 20ml NH_4^+ (5 mg/L) or PO_4^{3-} (10 mg/L) solution, and concentrations of NH_4^+ and PO_4^{3-} were measured after being shaken at 25°C for 180 minutes. The above steps were repeated for 3 times, and the regeneration rates of M-C/ZC were calculated using the equation [11]:

$$R_n = \frac{q_n}{q_0} \times 100\% \quad [11]$$

where R_n is the regeneration rate of M-C/ZC adsorption of NH_4^+ or PO_4^{3-} after regenerating n times/cycles (n=1, 2 and 3); q_n is M-C/ZC adsorption of NH_4^+ or PO_4^{3-} after n times regeneration (mg/g); q_0 is M-C/ZC initial adsorption of NH_4^+ or PO_4^{3-} (mg/g).

2.10. Characterization method

The slag composition in CGS was determined by using an X-ray fluorescence analyzer (XRF, ZETIUM, PANalytical, Netherlands). The phase of CGS was measured by using an X-ray diffract meter (XRD-6100, Shimadzu Corporation). The parameters were set to copper target, voltage 40 kV, tube current 30 mA, scan rate 7°/min, scan step size 0.02°, 2θ range 10~80°. The morphology and particle size distribution of C/ZC before and after the modification were analyzed using a scanning electron microscope (SEM, JSM-7800F, JEOL) at a high voltage of 15kV. The element composition and content of C/ZC before and after the modification were analyzed using an energy dispersive spectrometer (EDS, Oxford X-max 80, spray gold type Pt). The surface groups of C/ZC before and after modification, M-C/ZC before and after adsorption, and M-C/ZC after regenerations were analyzed using a Fourier Infrared Spectrometer (FT-IR, Nicolet iS5, Thermo Fisher, USA). The specific surface area, pore volume, and pore diameter of CGS were characterized by using a fully automatic gas analyzer (BET, Autosorb-iQ-AG-MP, American Kangta). The carbon content in the C/ZC was determined by using an elemental analyzer (EA, Vario EL III, Element Company, Germany). The potential value of the material was measured using a Zeta potentiometer (ZN, ZS90, Malvern, UK).

2.11. Statistical analysis

All experiments were performed for three times. SPSS version 24 (IBM Corp, Armonk, NY, USA) was used for data analysis, and Origin Pro 2017 (OriginLab Corp. USA) was used to plot and fit kinetics and isotherms.

3. Results and Discussion

3.1. Characteristics of carbon/zeolite composite

When CGS was synthesized to the composite, the characteristic peaks of zeolite appeared (Fig. 1). The broad peak of 2θ =24.16° corresponded to the main characteristic peak of zeolite, and 2θ =13.89°, 18.78° and 27.50° were also characteristic peaks of zeolite. The 2θ =43.81° and 77.54° were the characteristic peaks of carbon, which may be derived from the crystallization of carbon produced by CGS itself. The measurement result from the elemental analyzer shows that the

carbon content in the composite was between 40 and 50%. Therefore, the composite made from CGS is carbon/zeolite composite (C/ZC). The $2\theta = 64.40°$ characteristic peak corresponded to an aluminosilicate compound ($Na(Si_2Al)O_6 \cdot H_2O$), which may be an intermediate product in the process of synthesizing zeolite. As shown in Fig. 1, there was no obvious difference in the XRD diffraction spectrum between C/ZC and M-C/ZC. The intensity of each peak of M-C/ZC showed a decreasing trend, indicating that the iron was successfully loaded on C/ZC and it resulted in the rougher characteristic peaks (Baskan and Pala, 2011; Xu et al., 2020).

The irregular unburned carbon and the spherical particles with smooth surface of CGS can be founded in Fig. 2a. The synthesized zeolite spheres with rough surface and rod-shaped packing crystals of C/ZC can be clearly observed in Fig. 2b. The morphology of M-C/ZC did not change (Fig. 2c). An energy dispersive spectrometer was used to analyze the elemental composition. As shown in Fig. 2d, it can be seen clearly that the zeolite balls were formed by the accumulation of rod-shaped crystals and the distribution of surrounding carbon. According to Fig. 2e, iron was loaded on M-C/ZC, indicating that the iron modification method successfully filled the micropores and active parts of the zeolite did not destroy the original structure (Maulana and Takahashi, 2018).

The specific surface area and pore volume of C/ZC decreased slightly (Table 2), which may be due to the destruction of the carbon structure of CGS by the acid treatment. After iron modification, the specific surface area increased, similar to previous findings of iron-modified zeolite (Baskan and Pala, 2011). The specific surface area of M-C/ZC in this study reached 348.3 m^2/g, much higher than the 18.7 m^2/g of natural zeolite and 79.277 m^2/g of the same type of iron-modified zeolite (Baskan and Pala, 2011; Liu et al., 2017).

3.2. Adsorption capacity of ammonia nitrogen and phosphate of carbon/zeolite composite

CGS, C/ZC and M-C/ZC have shown the adsorption capacity of NH_4^+ (Fig. 3a, 3b, and 3c), but only M-C/ZC can adsorb PO_4^{3-} (Fig. 3d). The fitted Langmuir equation and Freundlich equation are shown in Fig.3, and the parameters of each fitting model are summarized in Table 3. According to the correlation coefficient R^2, the adsorption of NH_4^+ and PO_4^{3-} by the three materials was fitted well with the Langmuir adsorption isotherm. This indicates that NH_4^+ and PO_4^{3-} were adsorbed on the three materials through a single-layer adsorption process. The value of 1/n was less than 1, indicating that the adsorption process mainly involves chemical adsorption (Xu et al., 2020).

The maximum adsorption capacities of NH_4^+ of CGS and C/ZC were 3.84 mg/g and 5.17 mg/g, respectively (Table 3). After iron modification, the adsorption capacity of NH_4^+ of M-C/ZC increased to 7.44 mg/g, similar to the adsorption capacities of NAT-Z (7.09 mg/g) and iron-modified zeolite (IM-Z 6.83 mg/g) (Zhan et al., 2019), and better than biochar produced by pine sawdust (5.38 mg/g) (Yang et al., 2018). This indicates that C/ZC and M-C/ZC both have a good affinity towards NH_4^+-N, and

306 the iron coating on M-C/ZC has higher NH_4^+-N adsorption capacity. In addition, the
307 adsorption capacity of PO_4^{3-} by M-C/ZC reached 6.94 mg/g. Zhan et al. (2019) found
308 that the maximum P adsorption capacities by IM-Z predicted by the Langmuir
309 equation were 0.506 mg/g. Xu et al. (2020) demonstrated that the maximum P
310 adsorption capacities for iron oxide nanoparticles dispersed onto zeolite were
311 3.47mg/g. Therefore, the maximum adsorption of PO_4^{3-} by M-C/ZC was higher than
312 those by iron-modified zeolite. In addition, the adsorption of PO_4^{3-} by M-C/ZC is far
313 better than the rice husk ash (0.736 mg/g) (Mor et al., 2016).

314 *3.3. Surface groups of carbon/zeolite composite*

315 The strongest absorption band of CGS appeared at 3250~3500 cm^{-1} (Fig. 4a),
316 due to the hydroxyl stretching vibration of the water molecules in the slag pores. A
317 broad band appeared at the wavenumber of 1000 cm^{-1} after synthesizing C/ZC. The
318 1040 cm^{-1} was a typical silicate glass ribbon, which moved to the latter probably due
319 to the alternating condensation of Si-O bonds and Al-O bonds, or the glass component
320 in the material reacted with NaOH to form a zeolite structure (Stevens et al., 2008; Yi
321 et al., 2016). The 994 cm^{-1} was caused by the asymmetric tensile vibration of the YO4
322 (Y = Si or Al) tetrahedron (Yao and Sun, 2012), indicating that silicon and aluminum
323 participate in the crystallization and form the zeolite lattice. After the C/ZC was
324 modified by iron, the hydroxyl characteristic peaks at 3580 cm^{-1} reduced and the
325 hydroxyl characteristic peaks at 2930 cm^{-1} disappeared, showing that iron
326 successfully loaded onto C/ZC.

327 Scholars have found that the characteristic peaks of the NH_4^+ appeared at 1435
328 cm^{-1} (Huang et al., 2014). As shown in Fig. 4b, a new vibration peak appeared at 1435
329 cm^{-1} for M-C/ZC, indicating that ammonium ion was adsorbed by M-C/ZC. There
330 was a hydroxyl peak at 2930 cm^{-1} after the adsorption of PO_4^{3-} by M-C/ZC; this
331 corresponds to the hydroxyl peak of C/ZC before modification, indicating that the
332 loaded iron played an important role in the process of PO_4^{3-} adsorption. The ligand
333 exchange of hydroxyl group bound by iron formed the inner-sphere Fe–O–P
334 complexes, playing an important role in the adsorption of PO_4^{3-} by M-C/ZC (Fu et al.,
335 2018). Iron can be hydrolyzed into Fe-OH bond in water, and exchange with PO_4^{3-} to
336 form $FePO_4^{2-}$ (Cao et al., 2016). According to Fig. 4b, the characteristic peaks of PO_4^{3-}
337 and HPO_4^{2-} appeared at 1004 cm^{-1} and 874 cm^{-1}, respectively. It can be inferred that
338 M-C/ZC underwent a chemical reaction during the PO_4^{3-} adsorption process (Huang
339 et al., 2014).

340 *3.4. Comparison of adsorption rate and characteristics of ammonia nitrogen and*
341 *phosphate of carbon/zeolite composite*

342 The adsorption of NH_4^+ by CGS, C/ZC and M-C/ZC quickly reached a near
343 equilibrium state within 40 minutes (Fig. 5a, 5b, 5c). The adsorption of PO_4^{3-} by
344 M-C/ZC also reached a near equilibrium state within 60 minutes (Fig. 5d).

345 As shown in Table 4, the correlation coefficients R^2 of pseudo-first-order kinetics
346 for the adsorption of NH_4^+ of CGS, C/ZC and M-C/ZC were 0.962, 0.956, and 0.979,
347 respectively. The correlation coefficients R^2 of pseudo-second-order kinetics for the

adsorption of NH_4^+ of CGS, C/ZC and M-C/ZC were 0.987, 0.989 and 0.994, respectively. Similarly, the correlation coefficient R^2 of pseudo-first-order kinetics and the pseudo-second-order kinetics of M-C/ZC for the adsorption of PO_4^{3-} were 0.969 and 0.996, respectively. The adsorption process of NH_4^+ and PO_4^{3-} by CGS, C/ZC and M-C/ZC were fitted well with the pseudo-second-order kinetic model, indicating that the adsorption process is mainly chemical adsorption, including cation exchange, complexation and precipitation (Wu et al., 2020).

3.5. Effect of M-C/ZC dosage on the adsorption capacities of ammonia nitrogen and phosphate

The removal rates of NH_4^+ and PO_4^{3-} grew with the increasing amount of M-C/ZC (Fig. 6), reaching the maximums of 88% and 99%, respectively. However, the adsorption amounts of NH_4^+ and PO_4^{3-} declined with the increasing amount of M-C/ZC, indicating that adding a large amount of adsorbent can lead to a decrease in the utilization efficiency of the adsorption site and the adsorption capacity. Generally, the intersection of adsorption rate and adsorption capacity was considered as the optimal dosage in this study. Therefore, the suitable dosages of M-C/ZC to remove NH_4^+ and PO_4^{3-} are 8.5 g/L and 10 g/L.

3.6. Effect of temperature on the adsorptions of ammonia nitrogen and phosphate by M-C/ZC

The ΔH^o of adsorption of NH_4^+ and PO_4^{3-} by M-C/ZC were 3.35 and 7.15 KJ/mol, respectively, indicating that the process is endothermic (Table 5). The $\Delta S^o > 0$ demonstrated that the disordered reaction increased and the disorder of the system exacerbated. The negative values of ΔG^o indicated that the adsorption was spontaneously favourable (Kizito et al., 2015). The values of ΔG^o tended to decrease with the increasing temperature, indicating that temperature increase is beneficial to adsorption (Xu et al., 2020).

3.7. Effect of pH on the removal efficiencies of ammonia nitrogen and phosphate by M-C/ZC

As shown in Fig. 7a, the removal efficiency of NH_4^+ by M-C/ZC increased when pH grew from 5 to 7. The exchange capacity of H^+ by zeolite was higher than that of NH_4^+, resulting in that the adsorption capacity of NH_4^+ by zeolite was not very ideal due to the competition adsorption point between H^+ and NH_4^+ (He et al., 2016). Therefore, the increasing removal efficiency of NH_4^+ by M-C/ZC under increasing pH (from 5 to 7) contributed to the decrease in H^+. According to Fig. 7b, the zeta potential gradually decreased, and the zero charge point appeared at about pH=4.5. This means that when pH<4.5, the surface of M-C/ZC is positively charged; and when pH>4.5, the surface is negatively charged. There was more negatively charge of M-C/ZC when pH increased from 5 to 7, which benefited the adsorption of NH_4^+ positive charge. However, the removal efficiency of NH_4^+ by M-C/ZC decreased when pH > 7. This is probably due to that the NH_4^+ in the solution exists in the form of molecular NH_3, causing a decrease in adsorption capacity (He et al., 2016; Thornton et al., 2007). The negative charge on the M-C/ZC increased with increasing

pH, which resulted in decreasing adsorption of PO_4^{3-} (Fig. 7b). In addition, the higher concentration of OH^- in the higher pH solution hindered the ligand exchange between phosphate and hydroxyl(Yang et al., 2013), which resulted in the decrease in adsorption capacity of PO_4^{3-}.

3.8. Regeneration performance of modification of carbon/zeolite composite

After being regenerated for the first cycle, M-C/ZC regeneration rate of NH_4^+ was 95.23%; after the third cycle, the regeneration rate was still 76.96% (Fig. 8a). This indicates that M-C/ZC can continue to exhibit strong adsorption capacity for NH_4^+ through regenerations. According to Fig. 8b, the -OH peaks at 3480 cm^{-1} and 1640 cm^{-1} continued to decrease with the increasing number of regenerations. Notably, the adsorption peaks of Si-O-Si and Si-O-Al at 1040 cm^{-1} and 468 cm^{-1} decreased. The broad aluminosilicate peak at 1040 cm^{-1} was separated after the third regeneration, indicating that the desorption of NH_4^+ caused a certain degree of damage to the zeolite structure and it caused a gradual decrease in the adsorption capacity of NH_4^+ (Doekhi-Bennani et al., 2021).

After the first cycle, M-C/ZC regeneration rate of PO_4^{3-} was 57.23%; after the third cycle, the regeneration rate decreased to 3.77% (Fig.8b), indicating the relatively poorer regeneration capacity of M-C/ZC for PO_4^{3-}. This is because the M-C/ZC adsorption of PO_4^{3-} mainly comes from the loaded iron. As shown in Fig. 8c, the -OH peak at 2930 cm^{-1} tended to increase with the increasing number of regenerations. According to Fig. 4a, the -OH peak at 2930 cm^{-1} disappeared after iron loading on C/ZC. This indicates that the amount of loaded iron on M-C/ZC decreased with the increasing regeneration time and this resulted in the decreasing M-C/ZC adsorption capacity for PO_4^{3-}.

3.9. Limitations and future research

Similar to most studies, there are some limitations in the current study. M-C/ZC is very effective in adsorbing NH_4^+ and PO_4^{3-} in the water system to prevent the eutrophication of natural water. However, the adsorption capacity of eutrophic substances in the field has yet to be verified. Wastewater has the characteristics of non-fixed pollutant concentration, complicated water flow conditions, and the presence of various other interfering impurities. In the future, therefore, it is important to conduct research on the control of pollutants in actual wastewater (such as rainwater retention systems, road flow, urban domestic sewage, and others). In addition, further studies need to gauge the management of adsorbed M-C/ZC, because improper disposal is likely to cause the adsorbed eutrophic substances to be released again into the environment (Yang et al., 2015).

4. Conclusion

In this work, the carbon/zeolite composite was successfully synthesized with coal gasification slag, and the iron modification method was applied to improve the adsorption performance of NH_4^+ and PO_4^{3-}. The main conclusions are as follows:

(1) The maximum adsorption capacities of M-C/ZC for NH_4^+ and PO_4^{3-} were 7.44 mg/g and 6.94 mg/g, respectively. The removal efficiencies of NH_4^+ and PO_4^{3-} can peak at 88% and 99% under initial NH_4^+ (5 mg/L) and PO_4^{3-} (10 mg/L)

concentration.

(2) The adsorption process of NH_4^+ and PO_4^{3-} was an endothermic reaction. The larger adsorption capacities of NH_4^+ and PO_4^{3-} appeared in neutral and acidic conditions, respectively.

(3) The adsorption of NH_4^+ and PO_4^{3-} by M-C/ZC was mainly chemical adsorption, which was consistent with the good fit to the pseudo-second-order kinetics.

(4) The regeneration capacity of M-C/ZC of NH_4^+ was stronger than that of PO_4^{3-}. After three cycles, the regeneration rate of M-C/ZC of NH_4^+ was 76.96%, while that of PO_4^{3-} was only 3.77%.

Declaration of competing interest

The authors declare no conflict of interest.

Acknowledgements

This work was supported the Key Laboratory of Agro-Environment in downstream of Yangze Plain, Ministry of Agriculture, P. R. China (AE2018001), Six Talent Peaks Project in Jiangsu Province (JNHB-057), Qing Lan Project (20161507) and NUIST-Reading Research Institute Pump-Priming Application.

References

Appiah-Hagan, E., Chen, Y.W., Yu, X., A. Arteca, G., Pizarro, J., Mercier, L., Wei, Q., Belzile, N., 2018. Simple and energy-saving modifications of coal fly ash to remove simultaneously six toxic metal cations from mine effluents. Journal of Environmental Chemical Engineering 6, 5498-5509.

Baskan, M.B., Pala, A., 2011. Removal of arsenic from drinking water using modified natural zeolite. Desalination 281, 396-403.

Cao, D., Jin, X., Gan, L., Wang, T., Chen, Z., 2016. Removal of phosphate using iron oxide nanoparticles synthesized by eucalyptus leaf extract in the presence of CTAB surfactant. Chemosphere 159, 23-31.

Doekhi-Bennani, Y., Leilabady, N.M., Fu, M., Rietveld, L.C., van der Hoek, J.P., Heijman, S.G.J., 2021. Simultaneous removal of ammonium ions and sulfamethoxazole by ozone regenerated high silica zeolites. Water Research 188, 116472.

Fang, H., Cui, Z., He, G., Huang, L., Chen, M., 2017. Phosphorus adsorption onto clay minerals and iron oxide with consideration of heterogeneous particle morphology. Science of The Total Environment 605-606, 357-367.

Fu, H., Yang, Y., Zhu, R., Liu, J., Usman, M., Chen, Q., He, H., 2018. Superior adsorption of phosphate by ferrihydrite-coated and lanthanum-decorated magnetite. Journal of Colloid Interface Science 530, 704-713.

Gibbs, M., Özkundakci, D., 2010. Effects of a modified zeolite on P and N processes

and fluxes across the lake sediment–water interface using core incubations. Hydrobiologia 661, 21-35.

Gu, Y.Y., Qiao, X.C., 2019. A carbon silica composite prepared from water slurry coal gasification slag. Microporous and Mesoporous Materials 276, 303-307.

He, Y., Lin, H., Dong, Y., Liu, Q., Wang, L., 2016. Simultaneous removal of ammonium and phosphate by alkaline-activated and lanthanum-impregnated zeolite. Chemosphere 164, 387-395.

Hermassi, M., Valderrama, C., Font, O., Moreno, N., Querol, X., Batis, N.H., Cortina, J.L., 2020. Phosphate recovery from aqueous solution by K-zeolite synthesized from fly ash for subsequent valorisation as slow release fertilizer. Science of The Total Environment 731, 139002.

Huang, H., Xiao, D., Pang, R., Han, C., Ding, L., 2014. Simultaneous removal of nutrients from simulated swine wastewater by adsorption of modified zeolite combined with struvite crystallization. Chemical Engineering Journal 256, 431-438.

Huo, Z., Xu, X., Lü, Z., Song, J., He, M., Li, Z., Wang, Q., Yan, L., 2012. Synthesis of zeolite NaP with controllable morphologies. Microporous and Mesoporous Materials 158, 137-140.

Iqbal, A., Sattar, H., Haider, R., Munir, S., 2019. Synthesis and characterization of pure phase zeolite 4A from coal fly ash. Journal of Cleaner Production 219, 258-267.

Khaleque, A., Alam, M.M., Hoque, M., Mondal, S., Haider, J.B., Xu, B., Johir, M.A.H., Karmakar, A.K., Zhou, J.L., Ahmed, M.B., Moni, M.A., 2020. Zeolite synthesis from low-cost materials and environmental applications: A review. Environmental Advances 2, 100019.

Kizito, S., Wu, S., Kirui, W.K., Lei, M., Lu, Q., Bah, H., Dong, R., 2015. Evaluation of slow pyrolyzed wood and rice husks biochar for adsorption of ammonium nitrogen from piggery manure anaerobic digestate slurry. Science of the Total Environment 505, 102-112.

Li, F., Liu, Q., Li, M., Fang, Y., 2018. Understanding fly-ash formation during fluidized-bed gasification of high-silicon-aluminum coal based on its characteristics. Energy 150, 142-152.

Li, J., Zheng, B., Chen, X., Li, Z., Yang, H., 2021. The Use of Constructed Wetland for Mitigating Nitrogen and Phosphorus from Agricultural Runoff: A Review. Water 13, 476.

Lin, J., Zhan, Y., Zhu, Z., 2011. Evaluation of sediment capping with active barrier systems (ABS) using calcite/zeolite mixtures to simultaneously manage phosphorus and ammonium release. Science of The Total Environment 409, 638-646.

Liu, S., Chen, X., Ai, W., Wei, C., 2019. A new method to prepare mesoporous silica

from coal gasification fine slag and its application in methylene blue adsorption. Journal of Cleaner Production 212, 1062-1071.

Liu, T., Wang, H., Zhang, Z., Zhao, D., 2017. Application of synthetic iron-oxide coated zeolite for the pollution control of river sediments. Chemosphere 180, 160-168.

Maulana, I., Takahashi, F., 2018. Cyanide removal study by raw and iron-modified synthetic zeolites in batch adsorption experiments. Journal of Water Process Engineering 22, 80-86.

Mor, S., Chhoden, K., Ravindra, K., 2016. Application of agro-waste rice husk ash for the removal of phosphate from the wastewater. Journal of Cleaner Production 129, 673-680.

Petrus, R., Warchol, J.K., 2005. Heavy metal removal by clinoptilolite. An equilibrium study in multi-component systems. Water Research 39, 819-830.

Qu, J., 2008. Research progress of novel adsorption processes in water purification: A review. Journal of Environmental Sciences 20, 1-13.

Reitzel, K., Andersen, F.O., Egemose, S., Jensen, H.S., 2013. Phosphate adsorption by lanthanum modified bentonite clay in fresh and brackish water. Water Research 47, 2787-2796.

Ren, Z., Jia, B., Zhang, G., Fu, X., Wang, Z., Wang, P., Lv, L., 2021. Study on adsorption of ammonia nitrogen by iron-loaded activated carbon from low temperature wastewater. Chemosphere 262, 127895.

Salimova, A., Zuo, J., Liu, F., Wang, Y., Wang, S., Verichev, K., 2020. Ammonia and phosphorus removal from agricultural runoff using cash crop waste-derived biochars. Frontiers of Environmental Science & Engineering 14, 1-13.

Stevens, R.W., Siriwardane, R.V., Logan, J., 2008. In Situ Fourier Transform Infrared (FTIR) Investigation of CO_2 Adsorption onto Zeolite Materials. Energy Fuels 22, 3070-3079.

Tang, Y., Guo, X., Xie, Q., Finkelman, R.B., Han, S., Huan, B., Pan, X., 2018. Petrological Characteristics and Trace Element Partitioning of Gasification Residues from Slagging Entrained-Flow Gasifiers in Ningdong, China. Energy & Fuels 32, 3052-3067.

Thornton, A., Pearce, P., Parsons, S.A., 2007. Ammonium removal from solution using ion exchange on to MesoLite, an equilibrium study. Journal of Hazardous Materials 147, 883-889.

Wang, M., Xie, R., Chen, Y., Pu, X., Jiang, W., Yao, L., 2018. A novel mesoporous zeolite-activated carbon composite as an effective adsorbent for removal of ammonia-nitrogen and methylene blue from aqueous solution. Bioresource Technology 268, 726-732.

Wang, Y., Jia, H., Chen, P., Fang, X., Du, T., 2020. Synthesis of La and Ce modified X

zeolite from rice husk ash for carbon dioxide capture. Journal of Materials Research and Technology 9, 4368-4378.

Wang, Z., Lin, Y., Wu, D., Kong, H., 2016. Hydrous iron oxide modified diatomite as an active filtration medium for phosphate capture. Chemosphere 144, 1290-1298.

Wu, Y.H., Ma, Y.L., Sun, Y.G., Xue, K., Ma, Q.L., Ma, T., Ji, W.X., 2020. Graded synthesis of highly ordered MCM-41 and carbon/zeolite composite from coal gasification fine residue for crystal violet removal. Journal of Cleaner Production 277, 123186.

Xu, Q., Li, W., Ma, L., Cao, D., Owens, G., Chen, Z., 2020. Simultaneous removal of ammonia and phosphate using green synthesized iron oxide nanoparticles dispersed onto zeolite. Science of The Total Environment 703, 135002.

Yang, H., Huang, X., Thompson, J. R., Flower, R. J. 2015. Enforcement key to China's environment. Science, 347, 834-835.

Yang, H., Wright, J.A., Gundry, S.W., 2012a. Boost water safety in rural China. Nature 484, 318.

Yang, H., Xie, P., Ni, L., Flower, R.J., 2012b. Pollution in the Yangtze. Science 337. 410.

Yang, H.I., Lou, K., Rajapaksha, A.U., Ok, Y.S., Anyia, A.O., Chang, S.X., 2018. Adsorption of ammonium in aqueous solutions by pine sawdust and wheat straw biochars. Environmental Science & Pollution Research 25, 25638-25647.

Yang, S., Zhao, Y., Chen, R., Feng, C., Zhang, Z., Lei, Z., Yang, Y., 2013. A novel tablet porous material developed as adsorbent for phosphate removal and recycling. Journal of Colloid and Interface Science 396, 197-204.

Yao, Y., Sun, H., 2012. A novel silica alumina-based backfill material composed of coal refuse and fly ash. Journal of Hazardous Materials 213-214, 71-82.

Yi, L., Yan, C., Zhang, Z., Wang, H., Wei, Z., 2016. A comparative study on fly ash, geopolymer and faujasite block for Pb removal from aqueous solution. Fuel 185, 181-189.

Zhan, Y., Yu, Y., Lin, J., Wu, X., Wang, Y., Zhao, Y., 2019. Simultaneous control of nitrogen and phosphorus release from sediments using iron-modified zeolite as capping and amendment materials. Journal of Environmental Management 249, 109369.

589 Table 1

590 Chemical compositions of CGS (wt.%).

Material	SiO_2	Al_2O_3	CaO	Fe_2O_3	Na_2O
CGS	50.09%	18.97%	15.18%	6.09%	3.42%
Medical stone	70.4%	15.5%	3.4%	4.1%	-

591

592 Table 2

593 Comparison of specific surface area, pore volume and pore diameter of CGS, C/ZC
594 and M-C/ZC

Materials	Specific surface （m^2/g）	Average pore volume （cm^3/g）	Average pore diameter （nm）
CGS	298.5	0.132	0.520
C/ZC	273.3	0.123	0.526
M-C/ZC	348.3	0.157	0.526

595

596 Table 3

597 Parameters of adsorption isotherm NH_4^+ and PO_4^{3-} by CGS, C/ZC, M-C/ZC

Categories	Parameter	Units	NH_4^+			PO_4^{3-}		
			CGS	C/ZC	M-C/ZC	CGS	C/ZC	M-C/ZC
Langmuir	q_{max}	mg/g	3.84	5.17	7.44	\	\	6.944
	K_L	L/mg	0.025	0.013	0.033	\	\	0.022
	R^2		0.990	0.989	0.993	\	\	0.990
Freundlich	K_f	mg/g	0.250	0.161	0.698	\	\	0.422
	1/n		0.516	0.624	0.449	\	\	0.526
	R^2		0.958	0.963	0.962	\	\	0.989

598

599

Table 4

Kinetic parameters of CGS, C/ZC, M-C/ZC adsorption for NH_4^+ and PO_4^{3-}

Categories	Parameter	Units	NH_4^+			PO_4^{3-}		
			CGS	C/ZC	M-C/ZC	CGS	C/ZC	M-C/ZC
Pseudo-first-order	q_e	μg/g	119.4	208.7	331.7	\	\	803.1
	k_1	min^{-1}	0.328	0.235	0.343	\	\	0.199
	R^2		0.962	0.956	0.979	\	\	0.969
Pseudo-second-order	q_e	μg/g	125.2	221.9	344.0	\	\	851.4
	k_2	g/mg/min	0.0051	0.0018	0.0022	\	\	0.0004
	R^2		0.987	0.989	0.994	\	\	0.996

Table 5

Thermodynamic parameters of M-C/ZC adsorption for NH_4^+ and PO_4^{3-}

	ΔH^0（KJ mol^{-1}）	ΔS^0（KJ mol^{-1}）	ΔG^0（KJ/mol）		
			298K	308K	318K
NH_4^+	3.35	0.0184	-2.120	-2.230	-2.487
PO_4^{3-}	7.15	0.0303	-1.878	-2.170	-2.485

Figure captions

Fig.1 XRD pattern of CGS, C/ZC and M-C/ZC. Z represented zeolite

Fig.2 SEM analysis of CGS (a), C/ZC (b) and M-C/ZC (c), and distribution of elements on C/ZC (d) and M-C/ZC (e)

Fig. 3 The adsorption isotherms for NH_4^+ by CGS (a), C/ZC (b), and M-C/ZC (c), and adsorption isotherm for PO_4^{3-} by M-C/ZC (d)

Fig.4 Infrared spectrum: (a) CGS, C/ZC and M-C/ZC, (b) before and after M-C/ZC adsorption of NH_4^+ and PO_4^{3-}

Fig.5 The kinetic model fitting diagram of CGS (a), C/ZC(b), M-C/ZC(c) adsorption of NH_4^+ and M-C/ZC(d) adsorption of PO_4^{3-}

Fig. 6 Effect of M-C/ZC dosage on adsorption and removal: (a) NH_4^+ and (b) PO_4^{3-}

Fig.7 Effect of pH on removal efficiencies of NH_4^+ and PO_4^{3-} (a), and Zeta potential value (b)

Fig. 8 Regeneration rate of M-C/ZC after three regeneration cycles (a), and infrared images of regenerated M-C/ZC adsorption of NH_4^+ (b) and PO_4^{3-} (c)

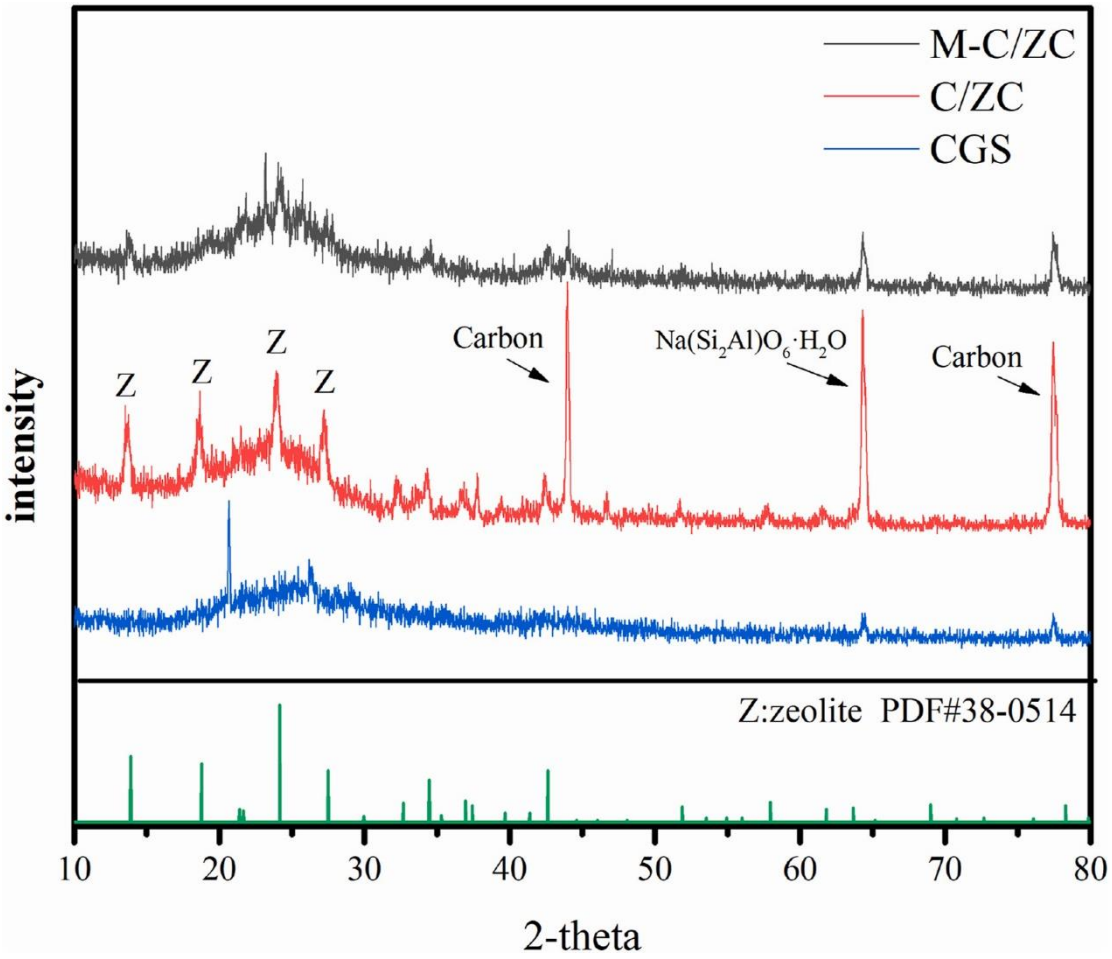

633

634 Fig. 1

635

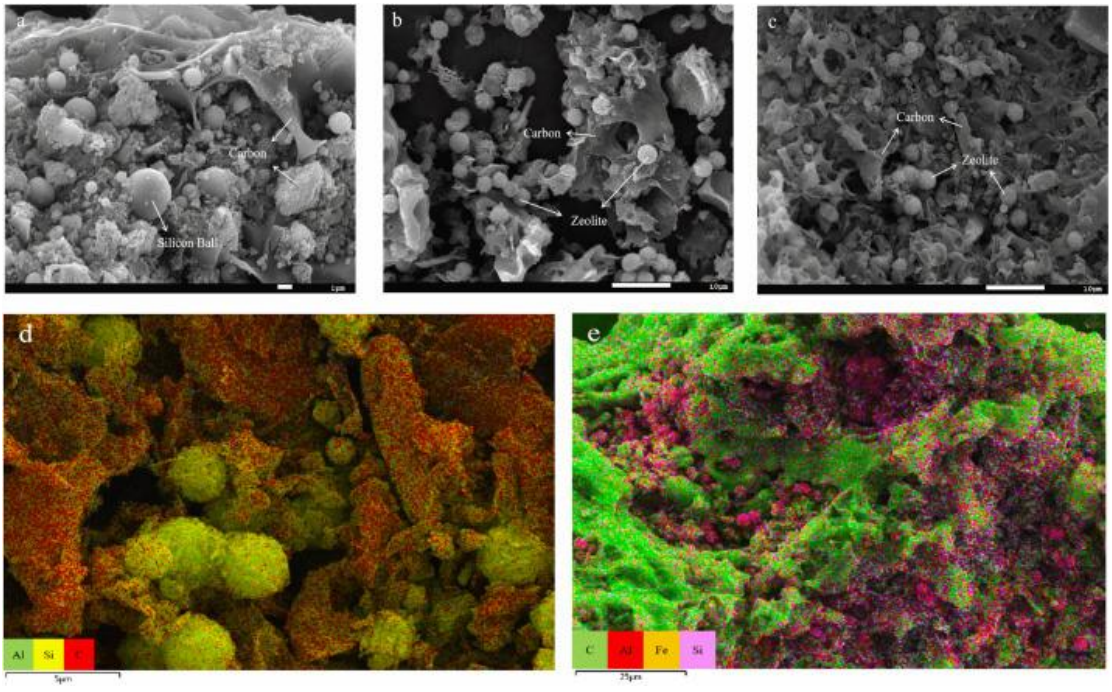

636

637 Fig. 2

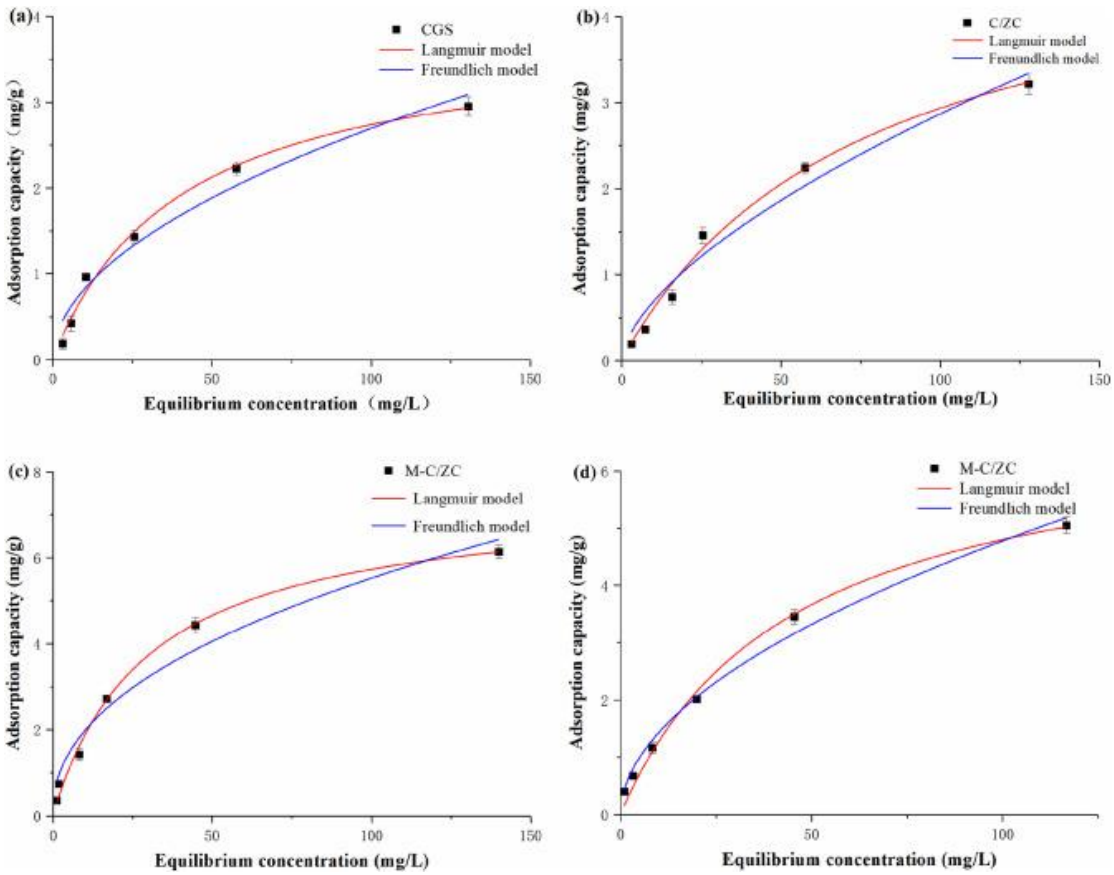

638

639 Fig. 3

640

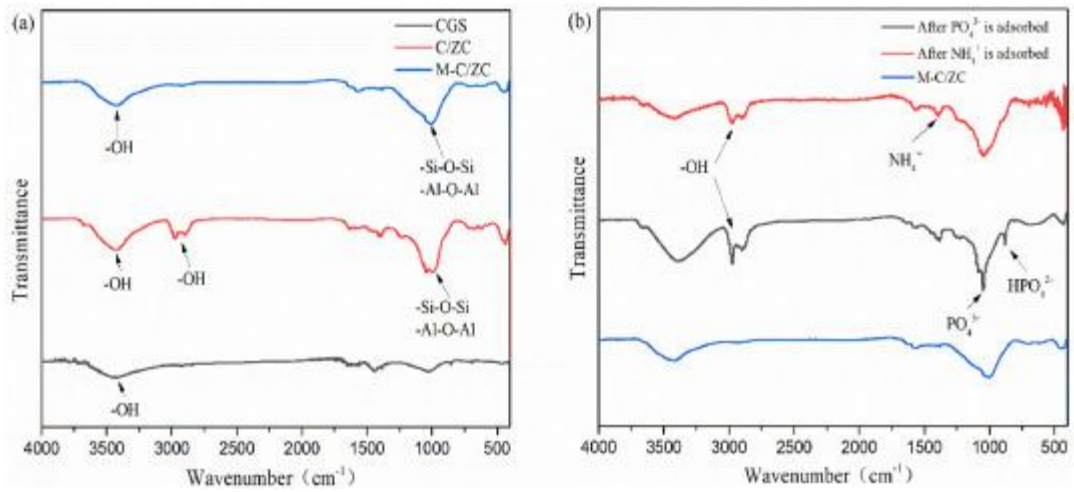

641

642 Fig. 4

643

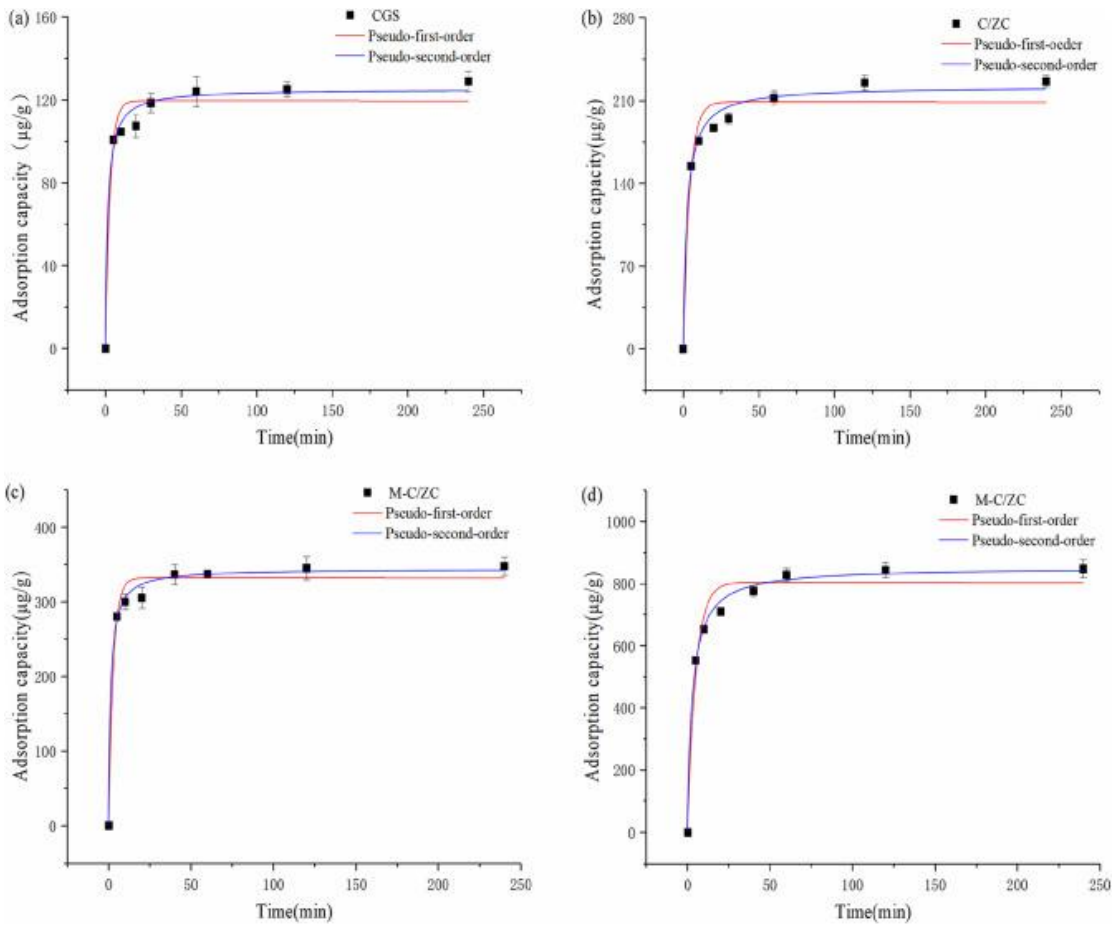

644

645 Fig. 5

646

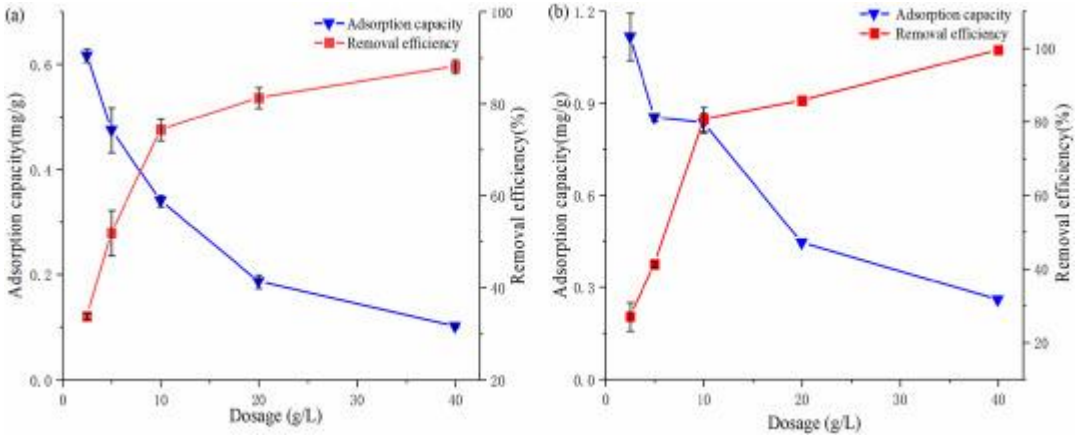

647

648 Fig. 6

649

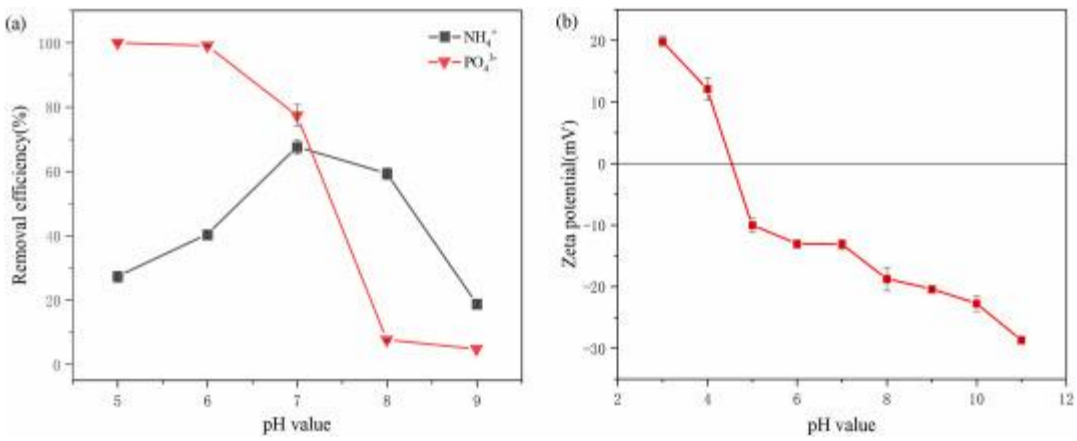

650

651 Fig. 7

652

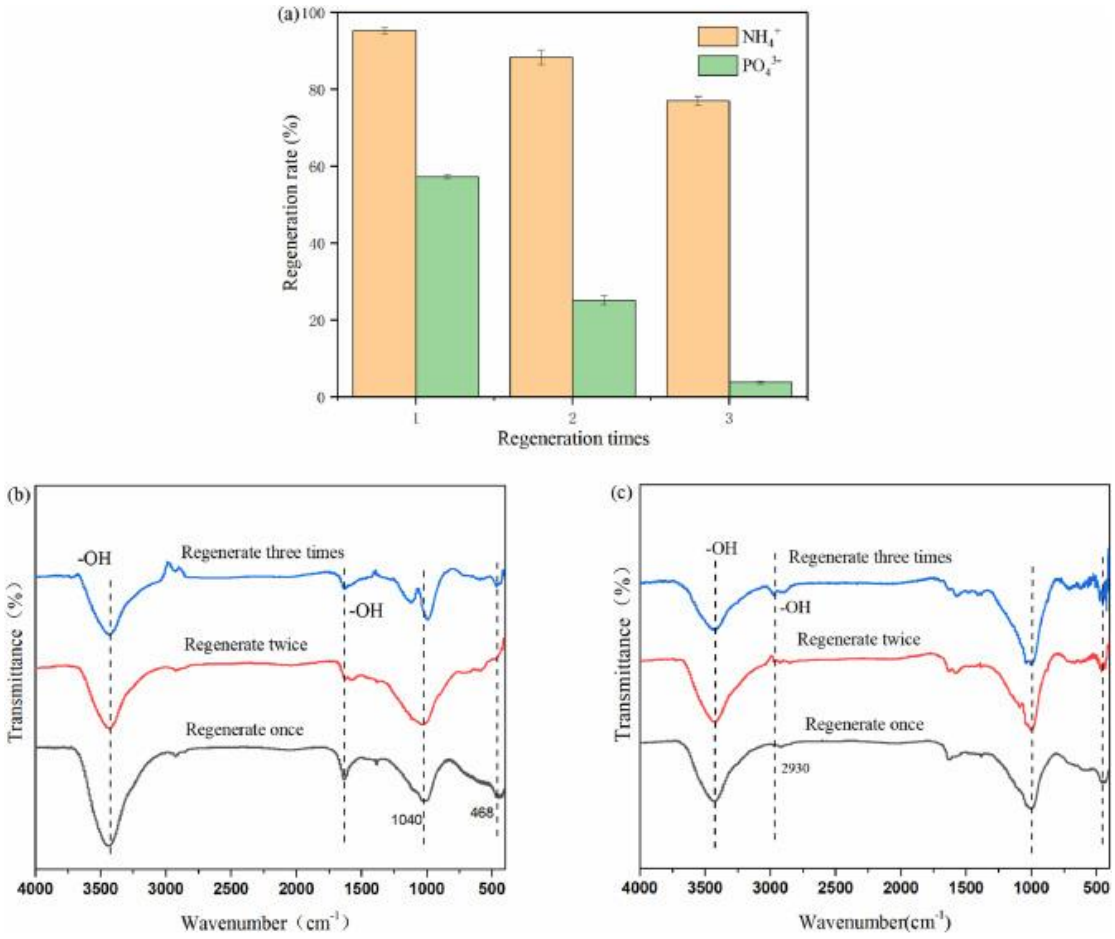

653

654 Fig. 8